

An investigation of the reduction mechanisms and magnesiothermic reactions in ZrC-Ni nanocomposite synthesis

Danial Davoodi^{a,b,*}, Morteza Tayebi^c, Amir Hossein Emami^d, Reza Miri^b, Saman Salahshour^d

^a Young Researchers and Elite Club, Najafabad Branch, Islamic Azad University, Najafabad, Iran

^b Kherad Sanat Arvand Company, Research and Development Unit, Engineering Department, Khorramshahr, Iran

^c Young Researchers and Elites Club, Science and Research Branch, Islamic Azad University, Tehran, Iran

^d Advanced Materials Research Center, Department of Materials Engineering, Najafabad Branch, Islamic Azad University, Najafabad, Iran

HIGHLIGHTS

- By increasing the graphite content in the initial powder mixture, the synthesis mechanism changed from combustion to gradual mode.
- Increasing the combustion time caused more progress in the synthesis.
- The pre-activation process resulted in the increase of the combustion time.
- Extra graphite acted as an inhibitor and resulted in the lengthening of the combustion time.
- By increasing the combustion time, the total synthesis time was reduced.

ARTICLE INFO

Keywords:

ZrC-Ni nanocomposite
Reduction mechanism
Pre-activation
Mathematical model

ABSTRACT

In the present study, the effects of preactivation stage and graphite content on the reduction and synthesis mechanisms of ZrO₂-NiO-Mg-graphite system were evaluated. For this purpose, the powder mixture with stoichiometric ratio was exposed to milling process. After the combustion it was found that the synthesis did not occur completely. By adding 10 wt% Mg to the mixture and further milling, the synthesis was completed and NiZr intermetallic compound was formed. Preactivation stage was carried out to complete the synthesis and reduction process of the composite samples. It was determined that after 6 h of preactivation, combustion time increased due to increase of oxide particles surface area and presence of graphite as a barrier between Mg and oxide particles. To confirm this, the mechanochemical process was performed with different graphite contents. It was realized that by increasing the graphite content as a postponing agent to levels higher than the stoichiometric limit, the synthesis was completed after 1200 min of milling without the presence of intermetallic compound.

1. Introduction

Cermets containing ZrC are among the ultra-high-temperature composites that provide elevated temperature strength, high hardness, thermal shock resistance, high modulus, and wear resistance [1–3]. Cermets are mainly used in aerospace industries, especially for solid-fueled rocket nozzle, engine parts, and cutting tools [3]. Utilization of high-temperature cermets as cutting tools causes thermal shocks and stresses when exposed to rapid temperature changes. Additionally, thermal stresses cause change in thermal expansion coefficients of

cermets with different components that results in thermal fatigue [4].

It was reported by Landwehr et al. [5–7] that thermal shock resistance of ZrC-Mo cermet increased by adding 30 wt% Mo to ZrC. In addition, Zhang and Liu [8] investigated the synthesis of TiC-ZrC-Co-Ni cermet. They prepared the cermet by milling the powder mixture for 24 h and sintering it at 1430 °C for 1 h. It was concluded that the thermal shock resistance enhanced due to the presence of the metallic phase.

By reviewing a number of different studies, it was discovered that existence of a metallic phase accelerated the formation of ceramic

* Corresponding author. Young Researchers and Elite Club, Najafabad Branch, Islamic Azad University, Najafabad, Iran.

E-mail addresses: Davoodi.danial@smt.iaun.ac.ir (D. Davoodi), Mortezatayebi95@yahoo.com (M. Tayebi), Dr.s.a.h.emami@gmail.com (A.H. Emami), miri_engineering@yahoo.com (R. Miri), saman.salahshour337@gmail.com (S. Salahshour).

<https://doi.org/10.1016/j.matchemphys.2018.10.014>

Received 23 May 2018; Received in revised form 23 September 2018; Accepted 7 October 2018

Available online 08 October 2018

0254-0584/ © 2018 Elsevier B.V. All rights reserved.

powder due to declining the melting point. Moreover, the presence of a metallic phase controls the size and morphology of the powder particles [9]. Zhang et al. [10] used the combustion of Co-Zr-B₄C powder mixture to synthesize the ZrC-ZrB₂ composite. In their study, Co controlled the size and morphology of the particles and its presence resulted in the formation of Co₂B and ZrCo₃B₂ phases during the synthesis. Their results revealed that increasing Co led to the decrease of the particle size and acceleration of ZrC and ZrB₂ formation.

In order to produce high temperature ceramics and their related composites, high purity nanosized powders, high chemical affinity between the starting materials and proper sintering ability of the materials are required [11]. So far, different techniques have been utilized for these ceramics. These methods include hot pressing [12,13], spark plasma sintering [14,15], in-situ reaction sintering [16,17], displacive compensation of porosity (DCP) [18,19], high temperature carbothermal reduction [20–22], solution-based processing [23–26], mechanical alloying [27–31] and solid-state metathesis route [32]. These techniques have been employed in different conditions which directly affect the mechanical properties. In the abovementioned techniques, ZrC has been usually used as a reinforcement phase where it plays the role of grain refiner and load transfer factor from matrix to reinforcement.

Xu et al. [33] synthesized ZrB₂-ZrC-Ni composite powder with the size of 50–75 μm after 6 h mixing of Ni-Zr-B₄C system via self-propagating high-temperature synthesis (SHS) method. Moreover, Landwehr et al. [6] reported that ZrC cermet with Mo matrix can be produced by hot pressing technique. They also found that by increasing the Mo content from 20 wt% to 40 wt%, the flexure strength and fracture toughness increased. In another investigation conducted by Zhang et al. [34], W/ZrC cermet was synthesized via DCP method with the fracture toughness seven times higher than pure ZrC.

In a similar vein, Lim et al. [20] used ZrO₂, C, and WC precursors to synthesize W/ZrC and W-Zr (CN) cermets. The cermets were prepared after 20 h of milling and heat-treating at 1300–1500 °C for 2 h and 1600 °C for 1 h under vacuum. Formation of isolated phases and coarse grains was considered as a problem, which occurred due to the application of conventional methods. The coarse carbide grains were refined by oxide phases which resulted in the change in thermal properties of the cermets [20,35,36].

In most of these methods, high temperature technology is required. According to the combustion during reaction in mechanically-induced self-sustaining reaction (MSR) method, this method was developed as a novel route. The MSR technique has been successfully utilized for preparation of ceramics, intermetallic compounds, and composites because of high-energy efficiency, short time, and low cost features. In this case, the conditions required for the production provide ultra-high cooling rate and formation of structural defects that offer availability of high chemical activity and ability of suitable sintering [11].

Further, Aoyon et al. [11] surveyed the ZrC synthesis through the SHS method and used nanosized ZrO₂ and magnesium powder and C₁₂H₂₂O₁₁ as the starting materials. ZrC was prepared after milling for 3 h, placement in oven at the temperature of 80 °C for 12 h and eventually heat treatment at 800 °C was applied for 10 min. In a different study, Davoodi et al. [37] synthesized ZrC by magnesiothermic method after milling for 30 h at low temperature without any heat treatment.

In the literature, to the best of our knowledge, there is no evidence of in-situ synthesis of ZrC-Ni cermet. In addition, it is evident that in most of the methods that are employed for synthesis of ZrC and its cermets, ultra-high temperature and high-tech equipment or MSR long time method are required; moreover, in both methods, the processes are costly.

In the present study, attempts were made to prepare high purity ZrC-Ni composite with nanosized particles using ZrO₂, NiO, Mg, and graphite raw materials via mechanochemical synthesis in the shortest possible time and without post-synthesis heat treatment.

Table 1
Properties of raw materials.

Material	Purity (%)	Particle size (μ)	Company
ZrO ₂	99.8	100	Merck
NiO	99.8	40	Merck
Mg	99	20	Merck
Graphite	99	5	Merck

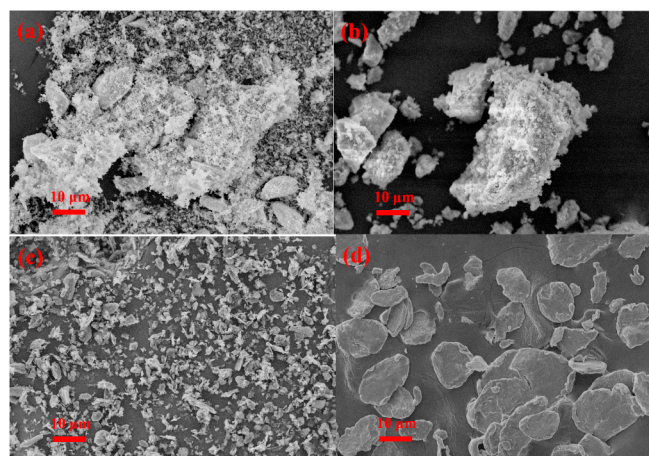
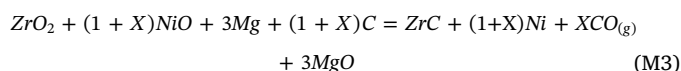
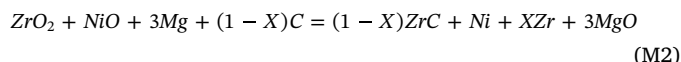
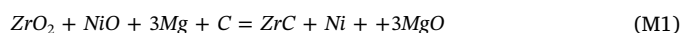


Fig. 1. Morphology of raw materials: (a) ZrO₂, (b) NiO, (c) graphite, and (d) Mg.

2. Experimental

2.1. Nanocomposite synthesis

A mixture of NiO, ZrO₂, Mg and graphite powders was used to synthesize ZrC-Ni nanocomposite according to M1, M2, and M3 reactions. Properties and morphologies of the raw materials are given in Table 1 and Fig. 1, respectively. The synthesis was carried out by milling process with powder-to-ball ratio of 1:20 at 600 rpm under argon (99.99% purity) atmosphere. To prevent the temperature elevation during milling, the ball mill was stopped every 45 min for 15 min.



In order to study the effective processes in the synthesis and reduction of ZrC-Ni composite two processes of pre-activation and graphite addition were employed in a way that pre-activation stage is referred as a process which the initial milled powders were milled to produce fine particles and increase of particle effective surface area and provide surface area for further processes.

2.2. Leaching process

In magnesiothermic reactions, Mg was employed as a reduction agent that reduced the oxide materials (ZrO₂ and NiO) and was converted into MgO which was a reaction byproduct. To remove this undesirable phase from the final powder, the leaching process was done by HCl 9% for 30 min at 80 °C [38].

2.3. Characterization

In order to characterize the phases, X-ray diffraction analysis (XRD,

Philips model PW30-40, Netherlands) was utilized at $2\theta = 10\text{--}80^\circ$ and step size of 0.05° under the voltage of 30 kV and 30 mA current. In all the experiments, Cu-K α irradiation ($\lambda = 1.5405 \text{ \AA}$) was used.

X'pert HighScore software was employed to determine the phases of the produced nanocomposite. To study the morphology and particle size of the prepared composite powder, scanning electron microscopy (SEM, Cam Scan model MV2300) and transmission electron microscopy (TEM, Philips model CM120, Netherlands) were utilized under the voltage of 120 kV.

2.4. Thermodynamic calculations

Prediction of thermodynamic behavior was carried out according to free energy, enthalpy of formation and adiabatic temperature of the reactions, and the obtained data were extracted from HSC Chemistry software (Version 5.0), according to Equation 1 [39].

$$\Delta Q = -\Delta H_{298}^\circ + \int_{298}^{T_m} \sum C_p(\text{Solid}). dT + \Delta H_m + \int_{T_m}^{T_{ad}} \sum C_p(\text{Liquid}). dT = 0 \quad (1)$$

Where, C_p , ΔH_{298}° , ΔQ and ΔH_m are specific thermal capacity, change of standard formation enthalpy at 298 °C, total heat of reaction and change of melt latent heat, respectively. Microstructural characterization included internal strain (due to the induced strains during the milling process) and the crystallite size of ZrC-Ni composite. These were calculated via Rietveld method in MAUD software, which was carried out using precise fitting of the XRD patterns. The precise fitting of the patterns was conducted by GoF function.

3. Results and discussion

3.1. Evaluation of thermodynamic behavior of possible reactions

In order to have a better understanding of thermodynamic conditions of possible reactions, the possibility of reaction occurrence was determined. Moreover, to predict the type of mechanochemical process from gradual or instant points of view, adiabatic theoretical temperatures of the reactions were calculated by thermodynamic data and type of reaction in the milling vial. Theoretical approach for the production of ZrC-Ni nanocomposite via mechanochemical process and using oxide raw materials can be divided into the following stages. It should be noted that the whole procedure has taken place in a fraction of a second after combustion in the milling vial.

3.1.1. Carbothermic reactions

In the presence of carbon, thermodynamically, reduction of NiO and ZrO₂ phases is not possible. The standard enthalpy and Gibbs free energy data for these reactions are shown in Table 2. These reactions are endothermic and their occurrence as MSR is not possible. In this case, each of the materials should be milled for long periods of time or a finalizing process such as heat treatment should be employed [40]. The

Table 2

Thermodynamic data of carbothermic reduction reactions.

No	Reaction	$\Delta G \left(\frac{\text{kJ}}{\text{mol}}\right)$	$\Delta H \left(\frac{\text{kJ}}{\text{mol}}\right)$
1	$ZrO_2 + 2C = Zr + 2CO(g)$	+768.173	+879.216
2	$ZrO_2 + C = Zr + CO_2(g)$	+648.143	+706.795
3	$ZrO_2 + 3C = ZrC + 2CO(g)$	+574.982	+682.567
4	$ZrO_2 + 2C = ZrC + CO_2(g)$	+454.951	+510.146
5	$ZrO_2 + C = ZrC + O_2(g)$	+849.315	+903.652
6	$NiO + C = Ni + CO(g)$	+74.433	+129.158
7	$2NiO + C = 2Ni + CO_2(g)$	+28.836	+85.895
8	$2NiO + ZrO_2 + 2C = 2Ni + Zr + 2CO_2(g)$	+676.979	+792.690
9	$NiO + ZrO_2 + 3C = Ni + Zr + 3CO(g)$	+842.607	+1008.374

ternary system of graphite, ZrO₂ and NiO have conditions similar to binary systems and oxide phase reduction is not practically accomplished by graphite.

In the presence of Mg, the conditions are different so that the reaction of NiO and ZrO₂ with Mg is highly exothermic. Regarding Table 3, reduction of NiO and ZrO₂ during milling is thermodynamically possible and releases 361900 J/mol and 102899 J/mol heat, respectively. The calculated adiabatic temperatures of the mentioned reactions were 3106 K and 1125.1 K, respectively. This shows the possibility of self-progressive synthesis reaction in high temperatures. If thermodynamic data for simultaneous presence of NiO and ZrO₂ with Mg are examined, it would be seen that in this system, the reaction is exothermic with adiabatic temperature of 2797.55 K and its spontaneous occurrence is possible during the milling process.

According to Table 4, after reduction of NiO and ZrO₂, their reactivity with graphite was investigated and it was found that the presence of ZrO₂ either in quaternary system or in ternary system can possibly form ZrC. The regarded reactions were both exothermic and their adiabatic temperatures of 2095 K and 3396 K showed their spontaneous occurrence, respectively.

3.2. Experimental study of the systems

The results of XRD analysis based on the stoichiometric ratio of M1 reaction after milling for different times (5, 60, 90, 300 and 600 min) are presented in Fig. 2. In the XRD pattern of the initial powder mixing (Fig. 2a), the peaks of ZrO₂, NiO, Mg, and graphite are evident. After milling for 1 h, the ZrO₂ peaks are still observed (Fig. 2b), but their intensities are reduced and the peaks are broadened due to fine powder particles, formation of crystalline defects, and increase of lattice strain [41]. The combustion happened after 90 min of milling which resulted in the appearance of MgO, ZrC, and Ni peaks in the pattern presented in Fig. 2c. As can be seen in this figure, the reaction did not completely occur because ZrO₂ peaks still remained in the pattern.

Another point here is the existence of Ni₂Zr₃ intermetallic phase in the system. According to reaction M1, ZrC should have been fully formed, but practically this did not occur because a part of reduced Zr had reacted with Ni in the combustion process instead of reacting with graphite according to proper conditions, which was due to the released heat and formed intermetallic compounds. It can be said that due to the combustion process, a part of graphite in the system turned into carbon monoxide (CO) instead of participating in the Zr + C = ZrC reaction (Eq. 13). As a result, the reaction did not fully occur. To complete the ZrC synthesis, 10 wt% Mg was added to the powder mixture after the combustion and the milling process was continued for 5 h.

According to Fig. 2d, it is evident that a part of ZrO₂ remained as a trace in the system and the synthesis did not completely occur. Also, it was observed that the peak intensities were significantly reduced and the peaks were broadened. This implies that the crystalline structure or the particle sizes reached to nanoscale dimensions. To complete the synthesis, 10 wt% Mg was again added to the powder mixture and the milling was continued for 10 h. According to Fig. 2e, it is obvious that the remained ZrO₂ was reduced by Mg and that it produced a composite consisting of ZrC, Ni, Ni₂Zr₃, and MgO phases.

The powder mixture was exposed to the leaching process after 10 h of milling in order to eliminate the MgO phase and the final composite consisting of ZrC-Ni-Ni₂Zr₃ was prepared (Fig. 3). Since the oxide particles were reduced by Mg particles, surface contact of oxide and Mg particles was essential. However, in this system, Mg and graphite particles randomly covered the surface of oxide particles and practically graphite acted as a barrier on the surface of oxide particles and prevented the contact of Mg and oxide particles. This process determined the time of combustion. In other words, by increasing the Mg contact with oxides, combustion took place faster. However, this was not true about the reaction progress. For better understanding of this process, a schematic has been illustrated in Fig. 4. By adding extra Mg after the

Table 3
Thermodynamic data of magnesiothermic reduction reactions.

No	Reaction	ΔG ($\frac{\text{kJ}}{\text{mol}}$)	ΔH ($\frac{\text{kJ}}{\text{mol}}$)	T_{ad} (K)
10	$\text{NiO} + \text{Mg} = \text{Ni} + \text{MgO}$	-357.769	-361.900	3106
11	$\text{ZrO}_2 + 2\text{Mg} = \text{Zr} + 2\text{MgO}$	-96.231	-102.899	1125.1
12	$\text{NiO} + \text{ZrO}_2 + 3\text{Mg} = \text{Ni} + \text{Zr} + 3\text{MgO}$	-454	-464.799	2797.555

Table 4
Thermodynamic data of the synthesis reactions.

No	Reaction	ΔG ($\frac{\text{kJ}}{\text{mol}}$)	ΔH ($\frac{\text{kJ}}{\text{mol}}$)	T_{ad} (K)
13	$\text{Zr} + \text{C} = \text{ZrC}$	-193	-196.8	3440
14	$\text{ZrO}_2 + 2\text{Mg} + \text{C} = \text{ZrC} + 2\text{MgO}$	-289	-299	2095
15	$\text{NiO} + \text{ZrO}_2 + 3\text{Mg} + \text{C} = \text{Ni} + \text{ZrC} + 3\text{MgO}$	-647.191	-661.447	3396

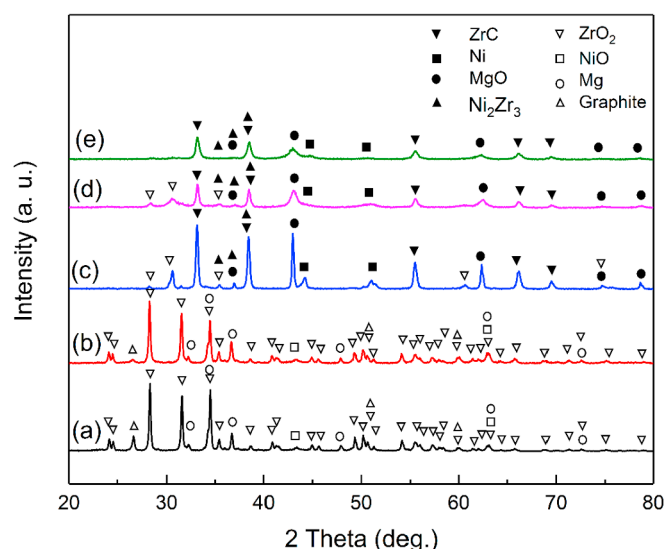


Fig. 2. XRD patterns of ZrO_2 , NiO , Mg and graphite powder mixtures after: (a) 5 min milling, (b) 1 h milling and combustion, (c) 1.5 h milling and combustion, (d) 5 h milling after combustion with extra 10 wt% Mg , and (e) 10 h milling after combustion with extra 10 wt% Mg .

combustion and according to the decrease of graphite content in the system (a part of it participated in ZrC formation in the combustion stage and the rest was turned into CO), the milling increased the possibility of Mg and oxide particles contact to complete the reduction.

3.3. The effect of pre-activation of the starting materials on the synthesis time

In order to examine the effect of pre-activation on the reaction time and progress, the oxide powders were milled for 3 h and 6 h. Early milling caused the NiO and ZrO_2 powders to be finer and increased the crystalline defects which resulted in the increase of effective surface area and activated the powder surfaces. After pre-activation, Mg and graphite were added to the powder mixture and milling was continued until the time of combustion. Schematic of pre-activation stage is presented in Fig. 5 for a better understanding. Combustion occurred after 100 min and 120 min for the samples which were pre-activated for 3 h and 6 h, respectively. It can be predicted that the increase of combustion time for 6 h pre-activated sample, as compared to 3 h pre-activated sample, was due to the fineness of oxide particles during milling. By reducing the size of these particles after addition of graphite and Mg to the system, since the graphite particles are finer than Mg particles, they covered the surface of oxides that resulted in less contact of Mg with the

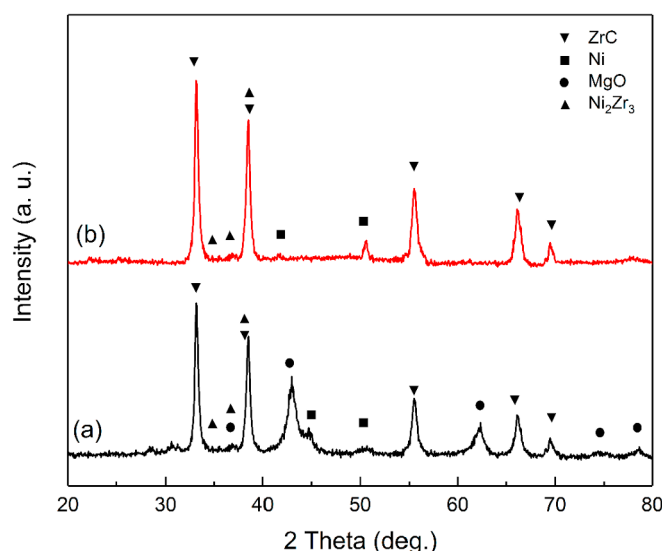


Fig. 3. XRD patterns of $\text{ZrC-Ni-Ni}_2\text{Zr}_3$ system: (a) before leaching and (b) after leaching.

oxides. This resulted in a more required time for combustion compared to both of the samples which were not pre-activated ($T_{\text{combustion}} = 90$ min) and the sample which was pre-activated for 3 h.

The XRD results in Figs. 6a and 7a show that the synthesis did not fully occur and ZrO_2 peaks were observable and the existence of Ni_2Zr_2 and Ni_7Zr_2 intermetallic compounds in the system was also confirmed. 10 wt% Mg was added to both samples and they were milled for 7 h. According to Fig. 6b, the XRD results show that although the intensities of ZrO_2 peaks were reduced, ZrO_2 still existed in the system. But according to Fig. 7b, it was observed that the synthesis was completed for the 6 h pre-activated sample, the ZrO_2 peaks were fully removed and a composite with ZrC , Ni , Ni_7Zr_2 and MgO was produced. This shows that by increasing the pre-activation time, the particles were refined; these particles contacted extra Mg in a secondary milling stage which completed the reduction process. This was not observed for the sample which was pre-activated for 3 h for the same finalizing milling time.

For better understanding of the mentioned mechanism in Fig. 5, at first the powder mixture of Mg , NiO and ZrO_2 was milled based on M2 reaction with different percentages of graphite ($X = 0, 0.25, 0.5, 0.75, 1$) and then the effect of graphite content on the combustion time was studied. As can be seen in Table 5 and Fig. 8, by increasing the graphite content, the combustion time increased, too.

The results showed that when the powder mixture was milled without graphite ($X = 1$), this opportunity was given to the oxide

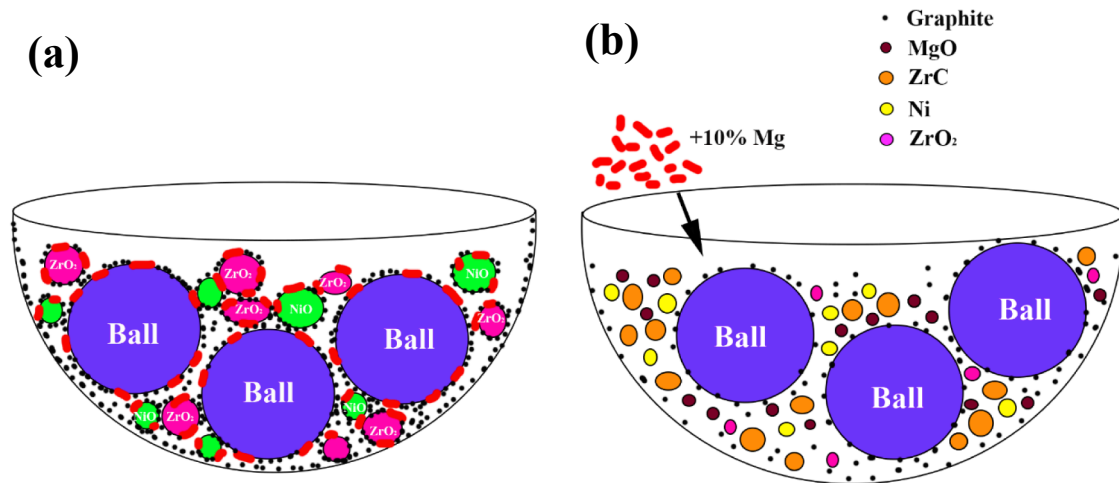


Fig. 4. (a) Contact schematic of oxide, Mg and graphite particles with stoichiometric ratio during milling, (b) schematic of extra Mg addition after initial milling to reduce the remaining ZrO₂ in the system during secondary milling.

powder to be in full contact with oxide particles and subsequently cause quicker combustion and the process time reduced to the minimum. By adding graphite to the powder mixture, graphite acted as a barrier and increased the required time for milling. By increasing graphite, its effect was more evident, so that for $X = 0.75$, the synthesis time practically increased by 1 min. But for $X = 0$, the combustion time increased by 64 min (schematic of the step-by-step addition of graphite is shown in Fig. 9).

3.4. Effect of adding extra graphite on the composite synthesis

The results showed that the most important factor in determination of the combustion time was the graphite content and its distribution in the system. By increasing the graphite content, graphite covered the particles surfaces, so for reduction of oxide particles, the particles should have been broken by the energy of the balls and the new created surface had contact with the Mg particles which finally increased the combustion time (Fig. 10). On the other hand, by increasing the combustion time, tendency of reduction for these particles increased due to the activation of oxide surfaces which caused more progression in the

reaction. Additionally, it can be said that a portion of graphite in M1 reaction turned into CO after the combustion and caused the ZrC not to be fully formed and lead to the creation of (Ni, Zr) intermetallic compounds. For this purpose and in order to study the effect of extra graphite in the system based on M3 reaction, the system was examined by adding extra 20 wt% and 30 wt% graphite.

Combustion occurred after 140 min for the sample which contained extra 20 wt% graphite. According to Fig. 11a, synthesis did not fully occur and there was no intermetallic compound present in the system. Synthesis continued without combustion for 600 min for the samples which contained extra 30 wt% graphite. The XRD patterns of these samples are presented in Fig. 11b. According to this figure, it is clear that synthesis partially occurred without combustion in the sample containing extra 30 wt% graphite. In fact, too high graphite content in the powder mixture caused the synthesis mechanism to change from combustion to gradual mode; i.e. due to high graphite content in the mixture, a great amount of Mg particles was not simultaneously allowed to have contact with the oxide particles and this prevented the combustion. Also, by locating the Mg particles against the oxide particles in small scale and the absorption of activation energy due to

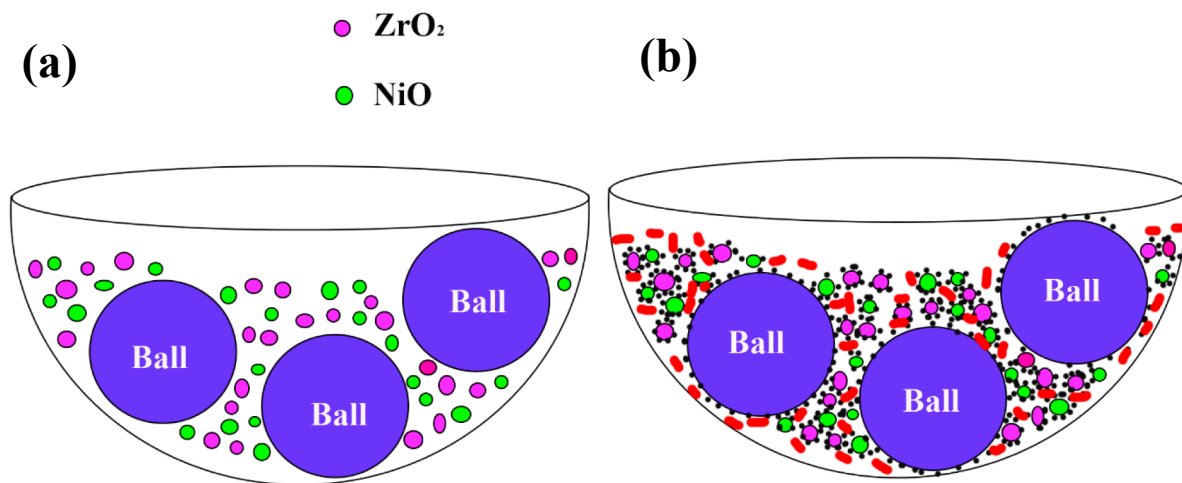


Fig. 5. Schematic of pre-activation process effect on contact of oxide, Mg and graphite particles: (a) pre-activation process which resulted in fine particles, (b) addition of graphite and Mg powders after pre-activation process and contact of graphite and Mg with oxide particles.

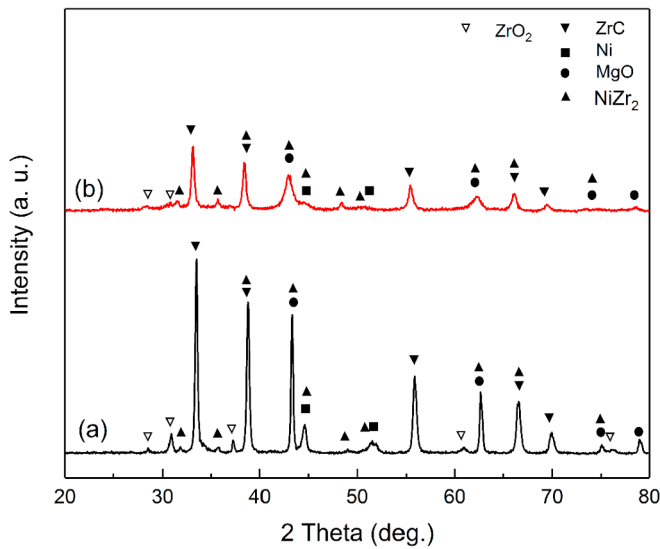


Fig. 6. XRD patterns of ZrO₂ and NiO powder mixtures which was milled for 3 h as pre-activation process: (a) after addition of Mg and graphite, milling for 100 min and combustion, and (b) 7 h milling after combustion with addition of extra 10% Mg.

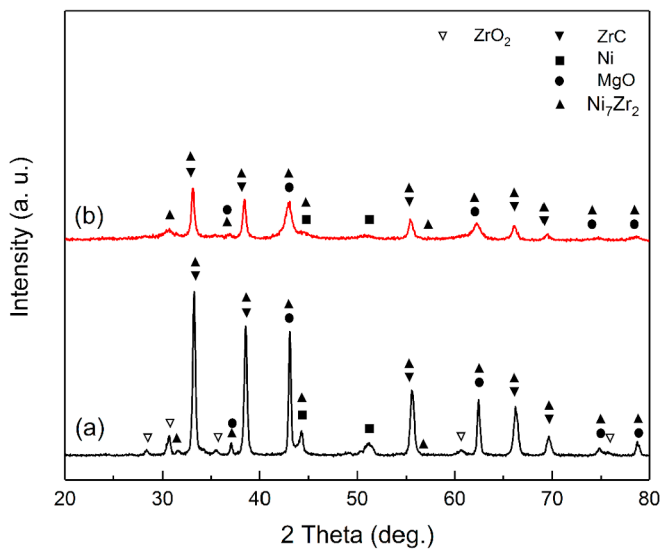


Fig. 7. XRD patterns of ZrO₂ and NiO powder mixtures which was milled for 6 h as per-activation process: (a) after addition of Mg and graphite, milling for 2 h and combustion, and (b) 7 h milling after combustion with addition of extra 10 wt% Mg.

Table 5
Variation of combustion time versus added carbon.

m _c (g)	0	0.072	0.144	0.216	0.288	0.35
t (min)	26	27	30	60	90	140

milling, reduction locally occurred and the released reduction heat resulted in localized synthesis plus provision of the essential activation energy for the adjacent particles.

Another powder mixture with similar conditions was exposed to milling for 1200 min and the synthesis was fully accomplished without formation of intermetallic compound (Fig. 11c). The XRD results after the leaching process of the prepared composite are illustrated in Fig. 12. This figure shows that MgO phase was completely removed from the system and ZrC-Ni composite was produced.

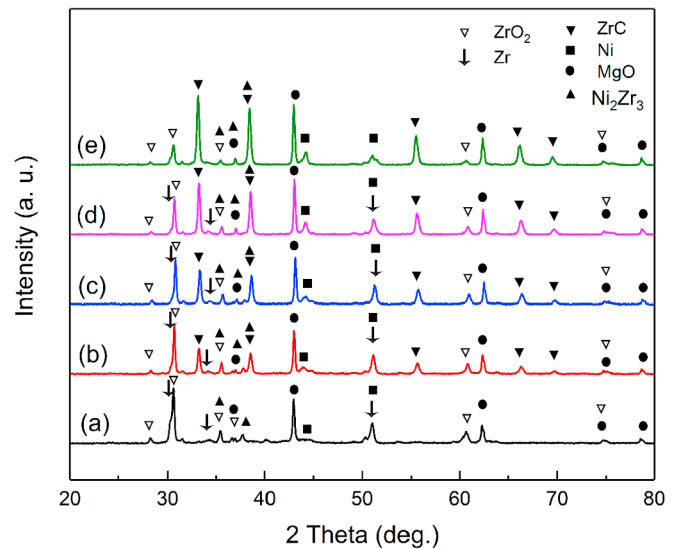


Fig. 8. XRD patterns of ZrO₂, NiO and Mg powder mixtures after: (a) 26 min milling, (b) after addition of graphite and milling for 27 min (1/4), (c) after addition of graphite and milling for 30 min (2/4), (d) after addition of graphite and milling for 60 min (3/4), and (e) after addition of graphite and milling for 90 min (4/4).

3.5. Proposing a mathematical model for description of relation between added graphite and combustion time

When no graphite was added to the mixture, t₀ exact time was needed. Consequently, mechanical energy was given to the raw materials to start the combustion reaction. By adding graphite, the required time for synthesis increased. This increase was related to the required time for diffusion of the reactants from the carbon layer around the particles which was named as t_D. Thus, the total time required for the initiation of combustion was named as t, which is the sum of these two time values:

$$t = t_0 + t_D \tag{2}$$

To calculate t_D, the following assumptions were considered:

- 1) The raw materials particles, except for graphite, were spherical with average radius of R.
- 2) Graphite surrounded the particles with a uniform layer with δ thickness.
- 3) The diffusion path (graphite layer) was assumed to be semi-infinite.

If m_c, V and ρ are the mass, volume and density of graphite layer, respectively:

$$m_c = \rho V \cong \rho(4\pi R^2\delta) \tag{3}$$

On the other hand, the diffusion depth of d in semi-finite path was determined by the following relation [42]:

$$d = a\sqrt{Dt_D} \tag{4}$$

Where D is the diffusion coefficient and a is a constant value which is dependent on the system geometry.

When d = δ, raw materials contact with each other in the combustion reaction. So:

$$m_c = \rho(4\pi R^2d) = 4\pi\rho aR^2\sqrt{Dt_D} \tag{5}$$

Or by arranging this equation, the result is:

$$t_D = \frac{1}{D} \left(\frac{m_c}{4\pi\rho aR^2} \right)^2 \tag{6}$$

Therefore, according to Eq. 2, the total required time for the

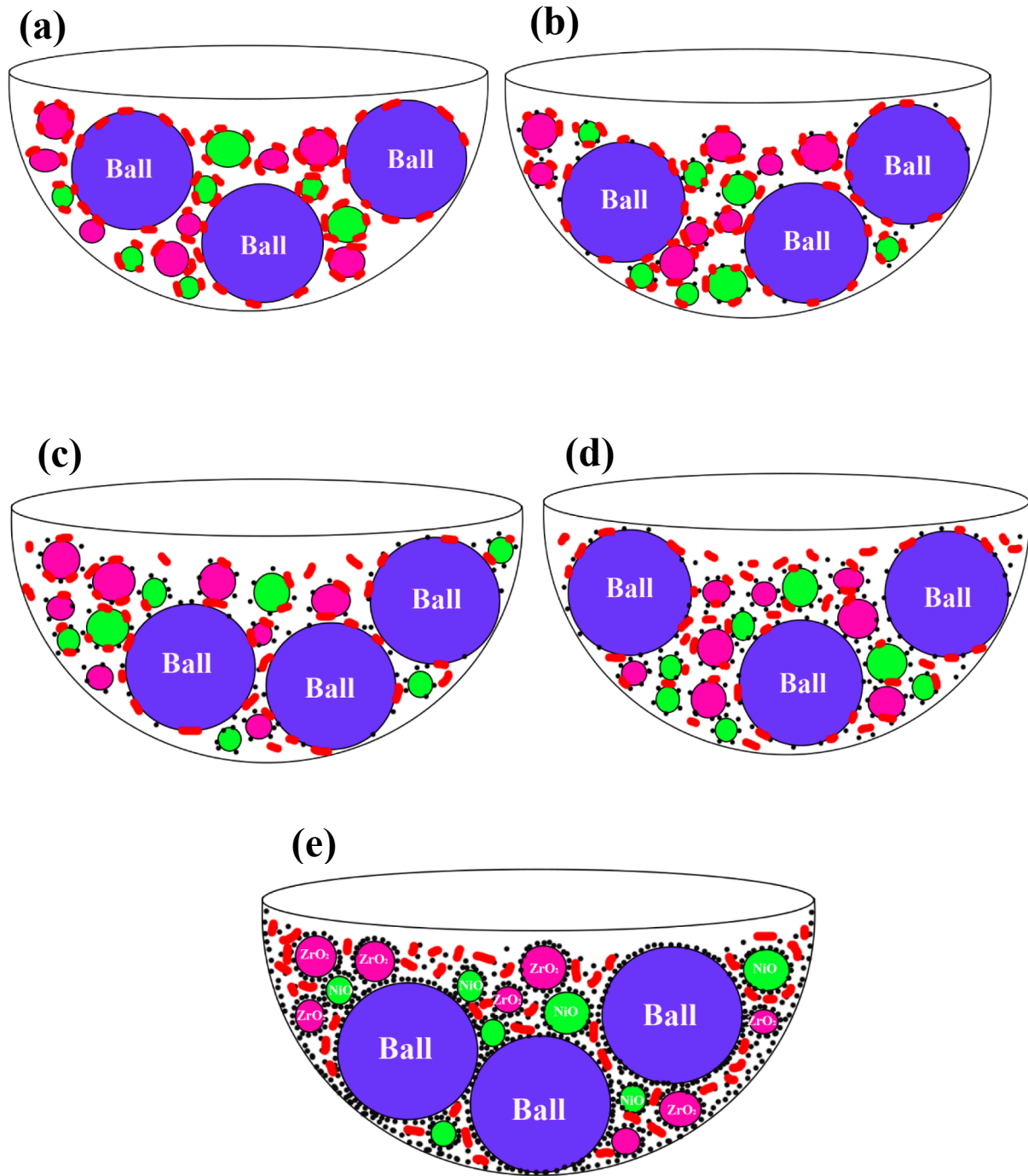


Fig. 9. Effect of graphite addition on particles contact in the systems of: (a) ZrO₂-NiO-Mg, (b) ZrO₂-NiO-Mg-1/4G Mg, (c) ZrO₂-NiO-Mg-2/4G, (d) ZrO₂-NiO-Mg-3/4G and (e) ZrO₂-NiO-Mg-G.

occurrence of combustion is:

$$t = t_0 + \frac{1}{D} \left(\frac{m_c}{4\pi\rho a R^2} \right)^2 \tag{7}$$

Table 5 lists the values of added graphite and the combustion time and in Fig. 13 experimental data were fitted with the model proposed in the present study. As can be seen in this figure, there is a proper conformity between these two values ($R^2 = 0.982$). The equation of fitted curve is:

$$t = 26 + 854.331 m_c^2 \tag{8}$$

3.6. Particle size and morphology of prepared composite

Rietveld method is based on modelling of XRD patterns using analytical function, relates the peak intensity to phase structure directly and presents a simulated pattern by analyzing microstructural parameters, peak shape, peak width and background parameters. In this method 2θ correction parameters, peak symmetry and peak broadening

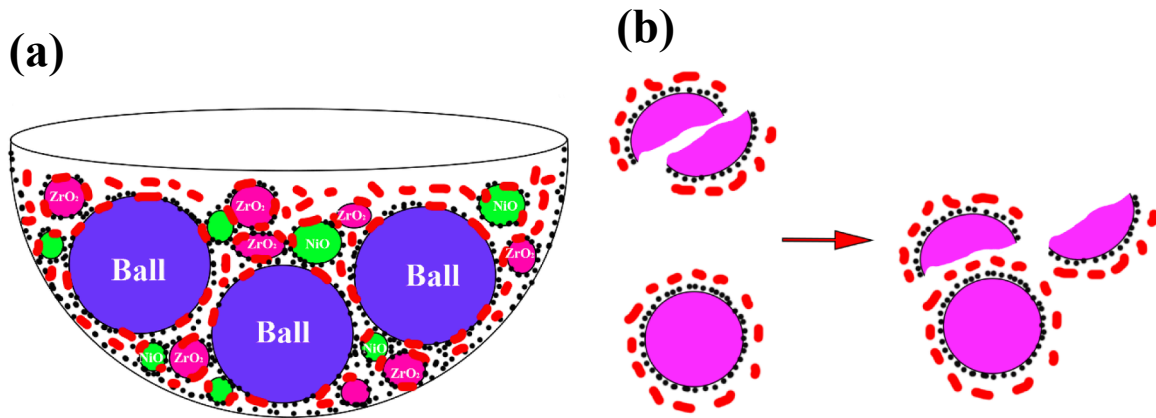


Fig. 10. (a) Schematic of particles contact in the powder mixture with presence of additional graphite, (b) reduction of oxide particles covered with graphite.

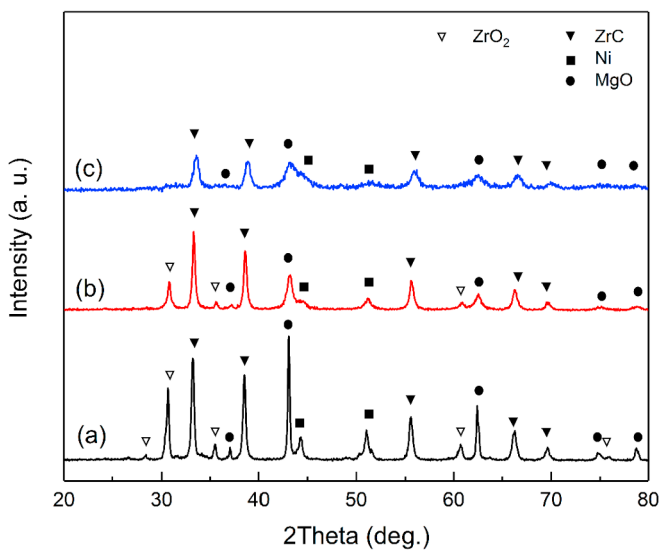


Fig. 11. XRD patterns of ZrO₂, NiO, Mg and graphite powder mixtures with addition of extra graphite: (a) 20 wt%, (b) 30 wt% and milling for 600 min, (c) 30 wt% and milling for 1200 min.

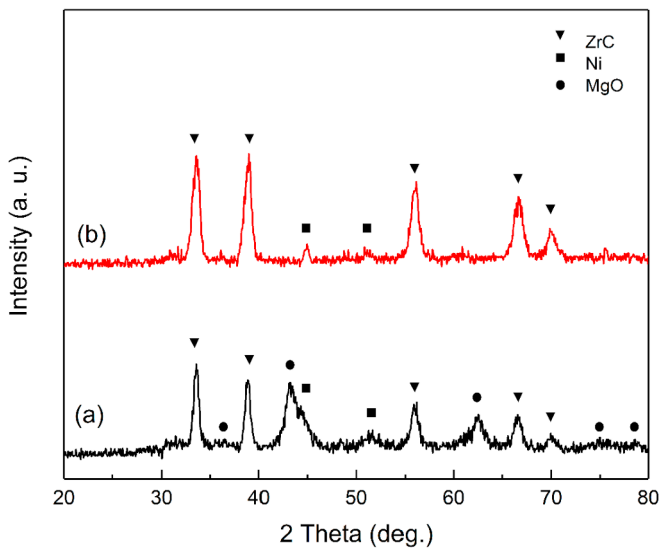


Fig. 12. XRD patterns of ZrC-Ni system: (a) before leaching, and (b) after leaching.

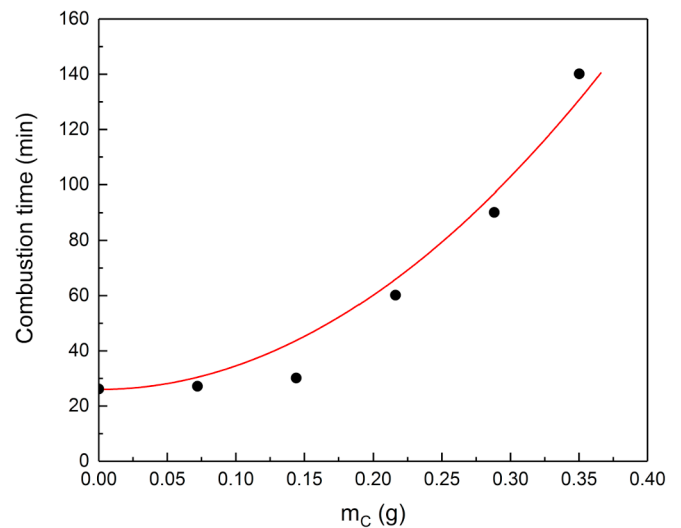


Fig. 13. Fitting of combustion time mathematical function based on added carbon with experimental data. Solid points represent experimental data and continuous line represents mathematical model.

Table 6
Crystallite size and lattice strain of synthesized composite.

		Crystallite size (Å)	Lattice strain
Composite synthesized from powder mixture M1	ZrC	410.45 ± 5	0.00251 ± 0.0005
	Ni	156.59 ± 2	0.00036 ± 0.0001
Composite synthesized from powder mixture M1 with preactivation	ZrC	354.66 ± 4	0.00113 ± 0.0005
	Ni	123.24 ± 6	0.00012 ± 0.00007
Composite synthesized from powder mixture M3 with 30% graphite over	ZrC	220.94 ± 5	0.00499 ± 0.0001
	Ni	80.08 ± 3	0.00030 ± 0.0002

are achieved based on reference sample. For this reason, crystallite size and internal strain of the powder particles are being calculated according to the extent of broadening and peak positioning.

The results of crystallite size and lattice strain determination for ZrC-Ni composite powder are brought in Table 6. As can be seen, the crystallite sizes varied from 8 nm to 15.6 nm for Ni and varied from 22 nm to 41 nm for ZrC, while the lattice strain differed from 0.00012 to 0.00036 and from 0.00113 to 0.00499 For Ni and ZrC, respectively. It can be seen that the lowest crystallite size was related to the

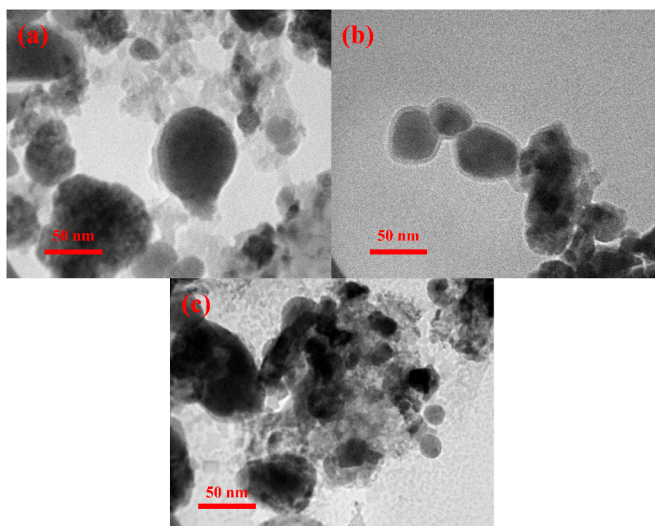


Fig. 14. TEM micrograph of synthesized composites by: (a) conventional synthesis, (b) synthesis with pre-activation stage and (c) synthesis with extra graphite.

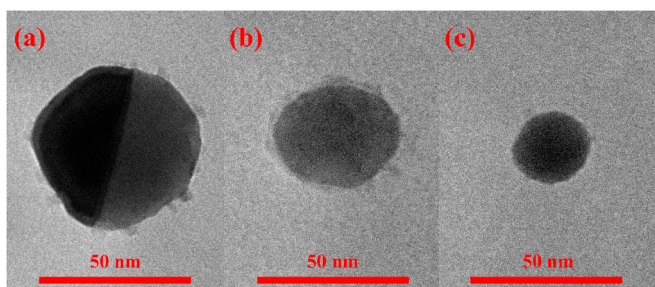


Fig. 15. TEM micrograph showing morphology of synthesized composites by: (a) conventional synthesis, (b) synthesis with pre-activation stage and (c) synthesis with extra graphite.

gradually synthesized sample.

ZrC-Ni composite powders obtained from 3 different synthesis procedures, i.e. conventional synthesis, synthesis with pre-activation, and gradual synthesis with extra graphite, were evaluated by TEM.

Fig. 14a displays that in conventional synthesis, the prepared sample had a particle size of 50 ± 5 nm with semi-spherical morphology (Fig. 15a). Fig. 14b is related to the sample which was synthesized by pre-activation stage; the figure shows finer particles in comparison with the samples which were synthesized by conventional synthesis, having a particle size of 42 ± 4 nm with spherical morphology (Fig. 15b). These results demonstrate that the pre-activation stage had a more significant effect on the fineness of produced particles rather than milling after combustion. According to Fig. 14c, among these three methods the composite powder produced by the gradual method had the smallest particle size (30 ± 3 nm). Furthermore, according to Fig. 15c, it is clear that morphology of the particles was entirely spherical. The reason for the formation of small sized particles was very long milling time (see Fig. 16).

4. Conclusions

Synthesis of ZrC-Ni nanocomposite powder by mechanochemical technique using ZrO_2 , NiO, Mg and graphite raw materials was successfully accomplished. Performing the milling at stoichiometric ratio of initial powder caused the combustion to occur after 90 min but synthesis was not fully achieved and Ni_2Zr_3 intermetallic compound plus ZrO_2 existed in the produced powder. Adding an extra 10 wt% Mg after combustion and secondary milling for 10 h resulted in the reduction of unreacted ZrO_2 and led to the completion of the synthesis.

After reduction of the oxide phases, Ni_2Zr_3 , $NiZr_2$ and Ni_7Zr_{12} intermetallic compounds were formed in the stoichiometric system due to appropriate conditions, insufficient amount of graphite in the system, and graphite conversion to CO.

Addition of extra graphite to the system caused the graphite particles to act like a barrier that resulted in postponing and completion of the process.

In addition to refining the initial oxide powders and activation of their surfaces, the pre-activation process resulted in covering more oxide particles due to their finer sizes. This, in effect, caused the graphite particles to act like a barrier between the oxide particles and Mg. This phenomenon postponed the reduction process that resulted in completion of the reduction process.

By adding extra graphite ($X = 0.3$) to the powder mixture, synthesis was completed without the presence of intermetallic compound during 1200 min.

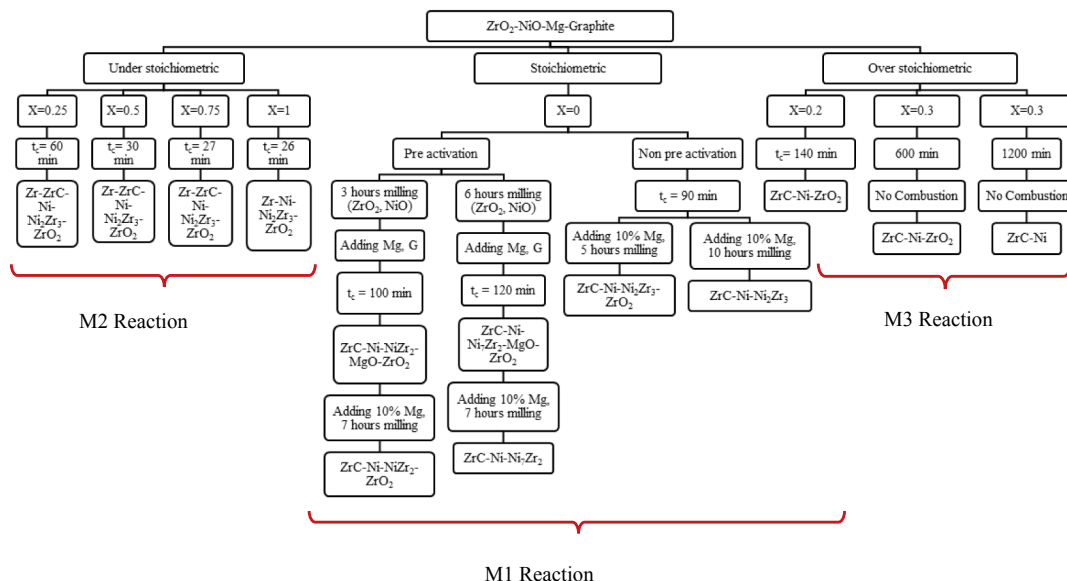


Fig. 16. Classification of reactions based on graphite percent.

References

- [1] A.L. Ortiz, V.M. Candelario, R. Moreno, F. Guiberteau, Near-net shape manufacture of B4C-Co and ZrC-Co composites by slip casting and pressureless sintering, *J. Eur. Ceram. Soc.* 37 (15) (2017) 4577–4584.
- [2] D. Yung, A. Zikina, I. Hussainova, H. Danninger, E. Badisch, A. Gavrilovic, Tribological performances of ZrC-Ni and TiC-Ni cermet reinforced PTA hardfacings at elevated temperatures, *Surf. Coating. Technol.* 309 (2017) 497–505.
- [3] Y. Yiping, W. Song, L. Wei, J. Jiming, Effect of ultra-high temperature heat treatment on microstructures of W/ZrC cermets fabricated by different routes, *Rare Metal Mater. Eng.* 46 (2017) 63–67.
- [4] C. Pan, D. Liu, C. Zhao, Q. Chang, P. He, Corrosion and thermal fatigue behaviors of TiC/Ni composite coating by self-propagating high-temperature synthesis in molten aluminum alloy, *Coatings* 7 (2017) 203, <https://doi.org/10.3390/coatings7110203>.
- [5] S.E. Landwehr, G.E. Hilmas, W.G. Fahrenholtz, I.G. Talmy, Processing of ZrC-Mo cermets for high-temperature applications, Part I: chemical interactions in the ZrC-Mo system, *J. Am. Ceram. Soc.* 90 (2007) 1998–2002.
- [6] S.E. Landwehr, G.E. Hilmas, W.G. Fahrenholtz, I.G. Talmy, S.G. Dipietro, Microstructure and mechanical characterization of ZrC-Mo cermets produced by hot isostatic pressing, *Mater. Sci. Eng.* 497 (2008) 79–86.
- [7] S.E. Landwehr, G.E. Hilmas, W.G. Fahrenholtz, I.G. Talmy, S. Wang, Thermal properties and thermal shock resistance of liquid phase sintered ZrC-Mo cermets, *Mater. Chem. Phys.* 115 (2009) 690–695.
- [8] X. Zhang, N. Liu, Effects of ZrC on microstructure, mechanical properties and thermal shock resistance of TiC-ZrC-Co-Ni cermets, *Mater. Sci. Eng., A* 561 (2013) 270–276.
- [9] Q. Lin, R. Sui, Wetting of carbide ceramics (B4C, SiC, TiC and ZrC) by molten Ni at 1753 K, *J. Alloy. Comp.* 649 (2015) 505–514.
- [10] M. Zhang, Y. Huo, M. Huang, Y. Fang, B. Zou, In situ synthesis and formation mechanism of ZrC and ZrB₂ by combustion synthesis from the Co-Zr-B4C system, *J. Asian Ceram. Soc.* 3 (2015) 271–278.
- [11] A. Da, F. Long, J. Wang, W. Xing, Y. Wang, F. Zhang, W. Wang, Z. Fu, Preparation of nano-sized zirconium carbide powders through a novel active dilution self-propagating high temperature synthesis method, *J. Wuhan Univ. Technol.-Materials Sci. Ed.* 30 (2015) 729–734.
- [12] T. Zhang, Y. Wang, Y. Zhou, G. Song, Effect of ZrC particle size on microstructure and room temperature mechanical properties of ZrCp/W composites, *Mater. Sci. Eng.* 527 (16–17) (2010) 4021–4027.
- [13] S. Guo, Densification, microstructure, elastic and mechanical properties of reactive hot-pressed ZrB₂-ZrC-Zr cermets, *J. Eur. Ceram. Soc.* 34 (3) (2014) 621–632.
- [14] W. Ji, J. Zhang, W. Wang, H. Wang, Z. Fu, Fabrication and properties of TiB₂-based cermets by spark plasma sintering with CoCrFeNiTiAl high-entropy alloy as sintering aid, *J. Eur. Ceram. Soc.* 35 (3) (2015) 879–886.
- [15] M. Radajewski, C. Schimpf, L. Krüger, Study of processing routes for WC-MgO composites with varying MgO contents consolidated by FAST/SPS, *J. Eur. Ceram. Soc.* 37 (5) (2017) 2031–2037.
- [16] S.C. Zhang, G.E. Hilmas, W.G. Fahrenholtz, Zirconium carbide-tungsten cermets prepared by in situ reaction sintering, *J. Am. Ceram. Soc.* 90 (2007) 1930–1933.
- [17] S. Ran, L. Zhang, O.V. der Biest, J. Vleugels, Pulsed electric current, in situ synthesis and sintering of textured TiB₂ ceramics, *J. Eur. Ceram. Soc.* 30 (4) (2010) 1043–1047.
- [18] S. Zhang, S. Wang, W. Li, Y. Zhu, Z. Chen, Microstructure and properties of W-ZrC composites prepared by the displacive compensation of porosity (DCP) method, *J. Alloy. Comp.* 509 (33) (2011) 8327–8332.
- [19] M. Adabi, A. Amadeh, A. Mohammadi, Effect of porosity content on composition of W/ZrC composites produced by displacive compensation of porosity (DCP) method, *Powder Metall.* 54 (2011) 320–324.
- [20] J. Lim, J. Kim, C. Park, S. Kang, Synthesis of W-ZrC and W-Zr(CN) cermets, The 18th International Conference on Composites Materials (ICCM), 2011 (Jeju Island, Korea).
- [21] M. Seo, S. Kang, Y. Kim, S.S. Ryu, Preparation of highly dispersed ultrafine ZrC by combination of carbothermal reduction of ball-milled ZrO₂ and C Mixture and bead milling, *Int. J. Refract. Metals Hard Mater.* 41 (2013) 345–350.
- [22] J. Dong, W. Shen, X. Liu, X. Hu, B. Zhang, F. Kang, J. Gu, D. Li, N. Chen, A new method synthesizing the encapsulated ZrC with graphitic layers, *Mater. Res. Bull.* 36 (5–6) (2001) 933–938.
- [23] J. Xie, Z. Fu, Y. Wang, S.W. Lee, K. Niibara, Synthesis of nanosized zirconium carbide powders by a combinational method of sol-gel and pulse current heating, *J. Eur. Ceram. Soc.* 34 (23) (2014) 13.e1-13.e7.
- [24] M. Dolle, D. Gosset, C. Bogicevic, F. Karolak, D. Simeone, G. Baldinozzi, Synthesis of nanosized zirconium carbide by a sol-gel route, *J. Eur. Ceram. Soc.* 27 (4) (2007) 2061–2067.
- [25] D. Zhao, H. Hu, C. Zhang, et al., A simple way to prepare precursors for zirconium carbide, *J. Mater. Sci.* 45 (23) (2010) 6401–6405.
- [26] C. Yan, R. Liu, Y. Cao, C. Zhang, D. Zhang, Synthesis of zirconium carbide powders using chitosan as carbon source, *Ceram. Int.* 39 (3) (2013) 3409–3412.
- [27] D. Lee, S. Jin, J. Yu, H. Lee, Synthesis of ultrafine ZrC powders by novel reduction process, *Mater. Trans.* 51 (12) (2010) 2266–2268.
- [28] T. Tsuchida, M. Kawaguchi, K. Kodaira, Synthesis of ZrC and ZrN in air from mechanically activated Zr-C powder mixtures, *Solid State Ionics* 101–103 (1997) 149–154.
- [29] H. Kwon, S.A. Jung, C.Y. Suh, W. Kim, Mechanical properties of (Ti_{0.9}W_{0.1}-x)C-Co cermet prepared by carbothermal reduction of high energy ball milled TiO₂-WO₃-C, *Ceram. Int.* 43 (2017) 1943–1947.
- [30] M. Jalaly, M. Tamizifar, M. Bafghi, F.J. Gotor, Mechanochemical synthesis of ZrB₂-SiC-ZrC nanocomposite powder by metallothermic reduction of zircon, *J. Alloy. Comp.* 581 (2013) 782–787.
- [31] J.Y. Xiang, S.C. Liu, W.T. Hu, Y. Zhang, C.K. Chen, P. Wang, J.L. He, D.L. Yu, B. Xu, Y.F. Lu, Y.J. Tian, Z.Y. Liu, Mechanochemically activated synthesis of zirconium carbide nanoparticles at room temperature: a simple route to prepare nanoparticles of transition metal carbides, *J. Eur. Ceram. Soc.* 31 (8) (2011) 1491–1496.
- [32] A.M. Nartowski, I.P. Parkin, M. MacKenzie, A.J. Craven, I. Macleod, Solid state metathesis routes to transition metal carbides, *J. Mater. Chem.* 9 (1999) 1275–1281.
- [33] J. Xu, B. Zou, S. Zhao, Y. Hui, W. Huang, X. Zhou, Y. Wang, X. Cai, X. Cao, Fabrication and properties of ZrC-ZrB₂/Ni cermet coatings on a magnesium alloy by atmospheric plasma spraying of SHS powders, *Ceram. Int.* 40 (2014) 15537–15544.
- [34] S.M. Zhang, S. Wang, W. Li, Y. Zhu, Z. Chen, Microstructure and properties of W-ZrC composites prepared by the displacive compensation of porosity (DCP) method, *J. Alloy. Comp.* 509 (33) (2011) 8327–8332.
- [35] M.B. Dickerson, P.J. Wurm, J.R. Schorr, W.P. Hoffman, P.G. Wapner, K.H. Sandhage, Near netshape, ultra-high melting, recession-resistant ZrC/W based rocket nozzle liners via the displacive compensation of porosity (DCP) method, *J. Mater. Sci.* 39 (2004) 6005–6015.
- [36] Y. Wang, Y. Zhou, G. Song, T. Lei, High temperature tensile properties of 30 vol. pct ZrCp/W composite, *J. Mater. Sci. Technol.* 19 (2003) 167–170.
- [37] D. Davoodi, S.A. Hassanzadeh-Tabrizia, A.H. Emami, S. Salahshour, A low temperature mechanochemical synthesis of nano structured ZrC powder by a magnesiothermic reaction, *Ceram. Int.* 41 (7) (2015) 8397–8401.
- [38] D. Davoodi, A.H. Emami, M. Tayebi, S.K. Hosseini, Rapid mechanochemical synthesis of nickel-vanadium carbide nanocomposite powder by magnesiothermic reaction, *Ceram. Int.* 44 (5) (2018) 5411–5419.
- [39] C.R. Bowen, B. Derby, Selfpropagating high temperature synthesis of ceramic materials, *Br. Ceram. Trans.* 96 (1997) 25–31.
- [40] B.R. Murphy, T.H. Courtney, Mechanochemically synthesized NbC cermets: Part I. Synthesis and structural development, *J. Mater. Res.* 14 (1999) 4274–4284.
- [41] C. Suryanarayana, Mechanical alloying and milling, *Prog. Mater. Sci.* 46 (2001) 1–184.
- [42] P. Shewmon, *Diffusion in Solids*, Springer International Publishing, 2017, <https://doi.org/10.1007/978-3-319-48206-4>.